

Low-temperature transport, thermodynamic, and optical properties of FeSi

S. Paschen, E. Felder, M. A. Chernikov, L. Degiorgi, H. Schwer, and H. R. Ott

Laboratorium für Festkörperphysik, Eidgenössische Technische Hochschule-Hönggerberg, 8093 Zürich, Switzerland

D. P. Young, J. L. Sarrao, and Z. Fisk

National High Magnetic Field Laboratory, Florida State University, 1800 East Paul Dirac Drive, Tallahassee, Florida 32306

(Received 9 May 1997)

We present a comprehensive series of electrical transport (conductivity, magnetoresistance, and Hall effect), thermodynamic (specific heat, magnetic susceptibility, and magnetization), and optical (reflectivity) measurements in varying temperature ranges between 0.05 and 330 K on high-quality FeSi single crystals grown by vapor transport. The entire set of data can consistently be described with the usual relations for a (compensated n type) semiconductor if an unconventional band structure is assumed. Compared to the results of mean-field band-structure calculations, the height of the peaks in the total density of states around the energy gap is considerably enhanced, implying enhanced effective masses. Most likely correlation effects are the source of these features. At very low temperatures we encounter metallic behavior. A low concentration of correlated itinerant charge carriers coexists with interacting magnetic moments. [S0163-1829(97)05043-1]

I. INTRODUCTION

The cubic $B20$ -type intermetallic compound FeSi, also frequently referred to as ϵ -FeSi, has been known since decades for its unusual thermodynamic properties at high temperatures.^{1,2} Above 100 K, the magnetic susceptibility rises rapidly with increasing temperature, passes through a maximum at approximately 500 K, and obeys a Curie-Weiss-type behavior at higher temperatures. Neutron diffraction,³ ²⁹Si NMR,⁴ and ⁵⁷Fe Mössbauer⁴ studies excluded, however, the onset of an antiferromagnetic order below 500 K. A similarly anomalous behavior was observed for the specific heat.² Its electronic component was reported to have a broad peak at around 200 K, which is roughly the temperature where the magnetic susceptibility increases most steeply with temperature.

The theoretical interpretation of these observations remains controversial. A number of different approaches have been suggested to explain these high-temperature properties of FeSi. A first approach uses a theory of itinerant-electron magnetism where FeSi is described as a nearly ferromagnetic semiconductor, the thermal and magnetic properties of which are strongly influenced by spin fluctuations with strongly temperature-dependent amplitudes.⁵⁻⁷ A second attempt calls upon a Kondo-lattice description.⁸⁻¹⁰ In this picture, the high-temperature magnetism is thought to arise from localized magnetic moments of Fe, which are not Kondo compensated above a certain critical temperature. This interpretation is of particular interest because of possible relations between correlated d - and f -electron systems. A third approach considers the concept of intermediate valence,¹¹ where the ground state is claimed to be $d^6\text{Fe}^{2+}$ hybridized with Si, leading to spin zero (the orbital momentum is quenched), and the lowest excited state is $d^7\text{Fe}^{1+}$ hybridized with Si, with spin $\frac{3}{2}$. The high-temperature magnetic behavior is thus explained by a thermally induced intermediate valence of Fe in FeSi. Yet another approach¹² describes FeSi with a two-band Hubbard model in the limit of large dimensions assum-

ing two symmetric tight-binding bands (the iron d bands) with a Hubbard term U acting within each band independently and with a moment independent hybridization. While for $U=0$ the ground state consists of doubly occupied states in the lower hybridized band, for $U\rightarrow\infty$ double occupancy is avoided. Related to this approach is a local-density-approximation (LDA)+ U band-structure calculation for FeSi.¹³ The anomalous behavior of the magnetic susceptibility and the specific heat of FeSi is claimed to be due to the proximity of a singlet semiconductor to ferromagnetic-metal transition in FeSi. It has, however, been argued¹⁴ that results similar to LDA+ U results are obtained if temperature dependences are included in the LDA band-structure calculations.

A central issue of all these models is the origin and the value of the energy gap in FeSi, a topic which has been addressed in a number of LDA band-structure calculations.¹⁵⁻¹⁹ All these reports give essentially the same results. The Fermi energy of FeSi is situated in a gap of the electronic excitation spectrum. The minimum-energy gap is indirect and between 0.05 and 0.11 eV, the minimum direct gap is approximately 0.14 eV. The calculated gap value is quite sensitive to small variations in the atomic positions of Fe and Si. As a result of several valence-band maxima and conduction-band minima occurring within a few meV of the gap edges, the total electronic density of states (DOS) rises rapidly on both sides of the gap. The gap is surrounded by two extremely narrow peaks of only approximately 50-meV width, mostly formed by Fe $3d$ states. These two peaks appear as particularly pronounced in Refs. 17 and 18. The peak above the gap is part of a wider structure of several 100-meV width. Fu, Krijn, and Doniach¹⁶ remarked that the dominating $3d$ character of the states around the gap is not what one would expect in a Kondo-insulator, where the gap results from a hybridization of localized $3d$ electrons with itinerant s or p electrons. On the other hand, Mattheiss and Hamann¹⁵ claimed that from their band-structure calculations they could not distinguish between a Kondo insulator and an en-

hanced spin-fluctuation model. Experimental gap values given in the literature^{2,9,20-24} range between 50 and 80 meV when extracted from electrical conductivity measurements, and between 60 and 100 meV when derived from magnetic-susceptibility and optical-reflectivity measurements, overall in relatively good agreement with the results of the above-mentioned calculations. It is known that LDA calculations usually underestimate the energy-gap value, but this notorious “band-gap problem” does not seem to appear in the case of FeSi. Jarlborg¹⁸ argued that this might be related to the gap occurring in the middle of the Fe 3*d* band in FeSi, and not between two different bands. This special feature of FeSi would also lead to an increase rather than the usual decrease of the gap width with pressure,¹⁸ as was indeed recently observed experimentally by Bauer *et al.*²⁵

The relevance of all these mean-field band-structure results for the real electronic structure of FeSi continues to be a topic of debate, however. Mattheiss and Hamann pointed out¹⁵ that, according to exact diagonalization studies on small many-body model systems,²⁶ the exact ground state is the analytic continuation of the noninteracting state, and that therefore the mean-field bands should be a relevant starting point for FeSi. Many-body effects can lead to an extreme renormalization of the LDA bandwidths, but only to a moderate renormalization of the LDA gap.

The relatively large amount of theoretical work aiming at explaining the high-temperature properties of FeSi is to be contrasted with much less theoretical work considering the low-temperature properties. These are often thought to be impurity dominated and therefore of little interest. We believe, however, that low-temperature properties can, even if impurity influenced or *because* they are impurity influenced, play an important role in clarifying the physical characteristics of FeSi. One example of a theoretical attempt to describe such a *real* physical system is the “dirty Kondo insulator” description of Schlottmann.²⁷⁻²⁹ In it, the effect of Kondo holes, i.e., of missing *f* or *d* electrons at a given site, on the DOS of a Kondo insulator is discussed and several low-temperature properties are predicted. Also Jarlborg,¹⁸ in the framework of an *ab initio* spin-polarized band theory for ϵ -FeSi, provided helpful indications on the expected influence of impurities on low-temperature properties. He points out that a local magnetic field, induced around a magnetic impurity in FeSi, can lead to spin polarization and a closing of the gap. This subsequently enhances the field because electrons from the minority valence band are transferred to the majority conduction band, a process which is most pronounced at low temperatures where the sharp rise in the DOS on both sides of the gap is not thermally smeared out. As a consequence, a sizable magnetic halo will be created around the impurity site.

In order to establish a reliable data base we have made a comprehensive series of electrical transport, thermodynamic, and optical measurements on high-quality single-crystalline FeSi samples below room temperature. All our experimental results are compatible with a description of FeSi being a semiconductor with an unconventional band structure, involving two narrow DOS peaks around the gap with an extremely high total DOS and considerably enhanced effective masses. At temperatures below 1 K, FeSi enters a metallic state in which interacting magnetic moments coexist with a

low concentration of itinerant charge carriers, a scenario interesting *per se*.

II. SAMPLES AND EXPERIMENT

We have measured the electrical resistivity, magnetoresistance, Hall effect, specific heat, magnetic susceptibility, and optical reflectivity in varying temperature ranges between 0.05 and 330 K on single-crystalline samples of FeSi. All transport measurements were made using the same crystal (which we will refer to as No. 1). For the specific-heat, magnetic-susceptibility, and optical-reflectivity measurements we used another crystal from the same batch to which we will refer as No. 2. Both samples were grown by vapor transport. The extremely high ratio of low temperature to room temperature resistivity of approximately 5×10^5 for No. 1 may be interpreted as an indication for a low defect concentration and a very high sample quality.

A. Structural characterization

We used several x-ray techniques to characterize our samples. In an energy dispersive x-ray microanalysis (EDX) of No. 2 we detected, besides Fe and Si, only spurious amounts of Cu, which are, most likely, due to backscattering from the microscope walls. We could not detect any foreign phase, i.e., inclusions which are chemically different from FeSi and which are larger than approximately 1 μm in diameter are unlikely to be present in the sample.

We analyzed a third crystal (No. 3) from the same batch as crystals Nos. 1 and 2 by powder diffraction at room temperature. Using an internal Si standard, the lattice constant was refined to $a = 4.4880(5)$ Å at room temperature. FeSi crystallizes with the cubic space group $P2_13$ and Fe and Si atoms are located at the special site $(4a)u, u, u$. Fixing the Fe and Si occupancy factor to 1.0, a Rietveld refinement yields, for the four equivalent Fe positions, $x/a = y/a = z/a = 0.137(2)$, and, for the four equivalent Si positions, $x/a = y/a = z/a = 0.842(3)$. If we fix only the Fe occupancy factor to 1.0 and refine the Si occupancy factor, we find a slightly better agreement with the experimental diffraction pattern. We then obtain a Si occupancy factor of 0.95(3), the Fe positions at $x/a = y/a = z/a = 0.139(2)$, and the Si positions at $x/a = y/a = z/a = 0.845(2)$. The corresponding sample stoichiometry is thus $\text{Fe}_{1+\delta}\text{Si}_{1-\delta}$ with $0.01 \leq \delta \leq 0.04$. The smallest δ value is just the maximum allowed silicon deficiency within the previously established FeSi homogeneity range.³⁰ For the higher δ values we would have to assume that locally some Fe rich phase exists. We analyzed this crystal (No. 3) by x-ray diffraction using the precession method prior to grinding it for the powder diffraction measurement. It consisted of at least four crystallites. Some of the excess Fe might, for example, have been situated at the grain boundaries.

Also crystal Nos. 1 and 2 were investigated by x-ray diffraction using the precession method. Each of them consists of at least two intergrown crystallites. The central region of crystal No. 1, which was investigated in the transport measurements, is, however, essentially single crystalline.

The implications of these structural investigations can be summarized as follows. Since FeSi is a cubic compound,

intergrown crystals are expected to have very similar physical bulk properties as single crystals. Only in samples consisting of many intergrown crystallites, grain boundaries might considerably influence intrinsic properties such as the spin susceptibility or the specific heat. Small deviations from the ideal 1:1 stoichiometry of Fe and Si are very difficult if not impossible to determine experimentally. The improved fit resulting from the Rietveld refinement when adjusting the occupancy factor of one of the constituents could also be due to the additional fit parameter. Therefore, one has to be extremely cautious when comparing results obtained from different samples, especially when synthesized by different methods.

B. Experimental techniques

Sample No. 1 was contacted with six gold wires using silver epoxy. The resistivity was measured between 0.07 and 300 K using a standard four-wire low-frequency ac technique. The magnetoresistance and the Hall effect were measured between 0.05 and 55 K by applying a dc current in external magnetic fields H of different magnitude up to $\mu_0 H = 7$ T. The magnetoresistance was measured in the so-called transverse configuration, that is, the magnetic induction B was perpendicular to the electrical current I . The current values were always checked to be in the ohmic regime. The magnetoresistance MR was extracted from the voltage V_1 measured along the current direction, the Hall voltage V_H from the transverse (i.e., perpendicular to I and B) voltage V_t , considering that MR is an even function of B and V_H is an odd function of B .

The specific heat of sample No. 2 was measured between 0.06 and 35 K using a relaxation-type technique, and the ac magnetic susceptibility of the same sample was measured between 0.05 and 1 K by a conventional mutual-inductance technique at a frequency of 420 Hz. Between 2 and 330 K, we measured the dc susceptibility using a moving-sample superconducting quantum interference device magnetometer. The absolute value of the ac susceptibility was determined by matching the data to that of the dc susceptibility. In addition, we measured the dc magnetization of sample No. 1 in external magnetic fields up to $\mu_0 H = 5$ T at various temperatures between 1.9 and 11 K.

The reflectivity spectrum $R(\omega)$ of sample No. 2 was measured as a function of temperature between 10 and 300 K over a very broad frequency spectral range, extending from the far infrared (FIR) up to the ultraviolet (UV), i.e., from 15 to 10^5 cm^{-1} . We made use of four different spectrometers. The FIR spectral range was covered with a Bruker IFS113v Fourier interferometer with an Hg arc light source and a He-cooled silicon bolometer detector. A fast scanning Bruker interferometer IFS48PC, a home-made spectrometer based on a Zeiss monochromator, and a commercial McPherson spectrometer were employed in the mid-infrared (mid-IR), visible, and UV spectral range, respectively. Below 5000 cm^{-1} , a gold mirror was used as reference. Moreover, the specimen was polished in order to obtain a suitable and shiny optical surface. The optical conductivity $\sigma_1(\omega)$ was obtained from Kramers-Kronig transformations applied to the measured optical reflectivity. Appropriate extrapolations were used above our highest-frequency limit, while from the

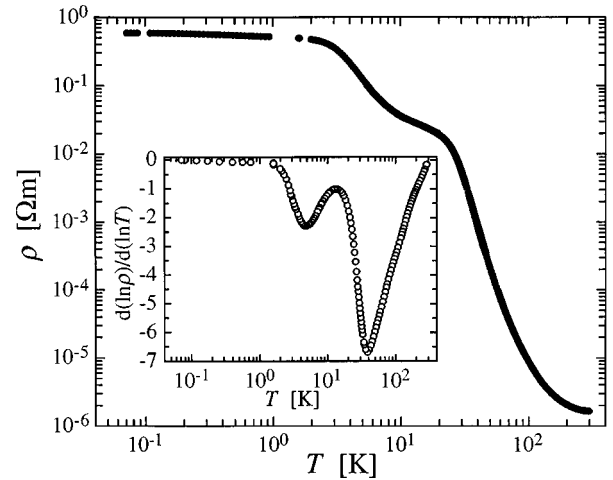


FIG. 1. Temperature variation of the electrical resistivity ρ of FeSi sample No. 1. The inset shows $d \ln(\rho)/d \ln(T) = (d\rho/\rho)/(dT/T)$.

FIR down to zero frequency the reflectivity was extrapolated with the Hagen-Rubens law between 300 and 100 K and to a constant value for the spectra monitored below 40 K.²⁴

III. EXPERIMENTAL RESULTS AND ANALYSIS

A. Transport

In Fig. 1 we show the temperature dependence of the resistivity ρ on a double-logarithmic plot. The resistivity at room temperature is, with 165 $\mu\Omega$ cm, well within the range of 140 – 280 $\mu\Omega$ cm previously reported for FeSi single crystals.^{9,21,23,31} Upon lowering the temperature, ρ increases by more than five orders of magnitude to 54.9 Ω cm at 0.07 K. In the inset of Fig. 1 we show $d \ln(\rho)/d \ln(T) = (d\rho/\rho)/(dT/T)$ as a function of T . The temperature derivative of ρ is negative over the whole covered temperature range. Above 200 K, ρ depends only weakly on T , but increases by more than three orders of magnitude between 200 and 30 K. The subsequent trend to saturation is followed by a second steep rise of ρ between approximately 15 and 5 K. At very low temperatures, $\rho(T)$ tends to saturate. Below 0.3 K, $\rho = \rho_0 - AT^2$ with $\rho_0 = 0.59$ Ω m and $A = 0.27$ Ω mK^{-2} is an adequate description of the data. The saturation of $\rho(T)$ to a finite value ρ_0 at very low temperatures is reflected in the trend $d \ln(\rho)/d \ln(T) \rightarrow 0$ as $T \rightarrow 0$.

In Fig. 2 we present the magnetoresistance data in the form $\text{MR} = [R(7T) - R(0)]/R(0)$ between 0.05 and 55 K. MR(T) is negative over practically the whole temperature range, reaching a maximum absolute value of approximately 12% around 7 K. Only between 30 and 45 K, is a small positive MR observed. Examples of isothermal MR(B) curves will be shown and analyzed in Sec. IV B.

The Hall effect was measured at several fixed temperatures between 1.5 and 55 K in external magnetic fields H up to $B = \mu_0 H = 7$ T, and at different temperatures between 0.1 and 1 K at up to 2 T. Only in two relatively narrow temperature ranges, namely, between 30 and 55 K and between 4 and 10 K, is the Hall resistivity $\rho_H = V_H d/I$ approximately a linear function of B , i.e., $\rho_H = R_H B$, where d is the sample thickness and R_H the Hall coefficient. The $\rho_H(B)$ curves in

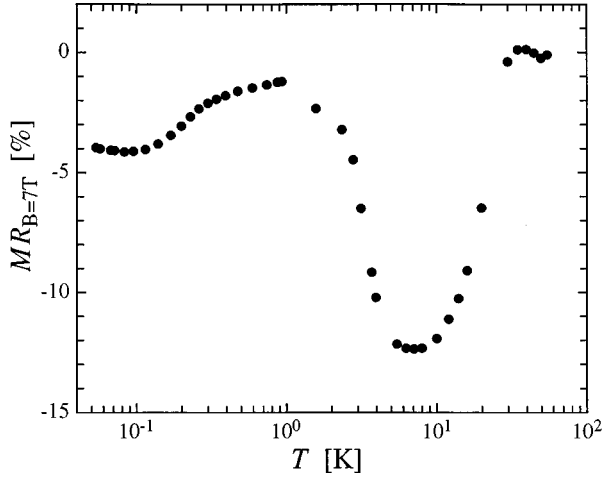


FIG. 2. Temperature dependence of the magnetoresistance $MR = [R(B) - R(0)]/R(0)$ of FeSi sample No. 1 measured in an external magnetic field H corresponding to $B = \mu_0 H = 7$ T.

these two regimes are shown in Fig. 3. The corresponding $R_H(T)$ values are shown later in Fig. 15(b). Between 30 and 55 K, R_H is positive, and between 4 and 10 K, R_H is negative. In the transition regime between 10 and 30 K, ρ_H behaves chaotically, and no reliable determination of R_H was possible. Below 4 K, $\rho_H(B)$ reveals pronounced nonlinearities, as shown in Fig. 4, and below 1 K, the transverse voltage $V_t(B)$ displays a hysteretic field dependence, as is shown in Fig. 5.

For the analysis of the nonlinear $\rho_H(B)$ curves, we consider the Hall effect due to two kinds of charge carriers, and the anomalous Hall effect due to the magnetic properties of the material. The field dependence of the Hall coefficient in a two-band model can be written in the form³²

$$R_H = \frac{R_0 + R_\infty \mu^2 B^2}{1 + \mu^2 B^2}, \quad (1)$$

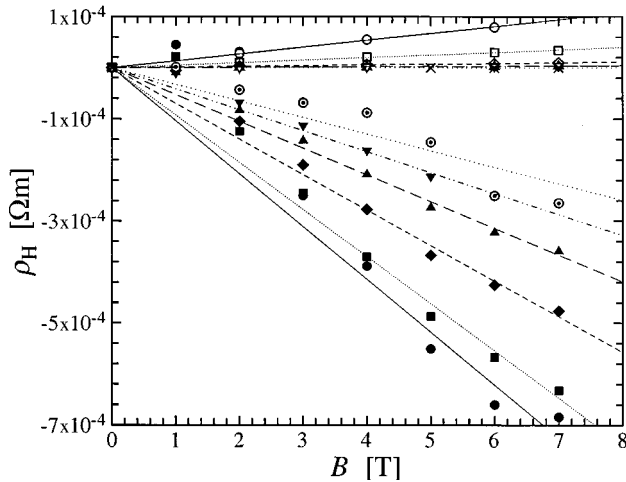


FIG. 3. Hall resistivity ρ_H vs external magnetic induction $B = \mu_0 H$ isotherms of FeSi sample No. 1. The dots are the data points, and the lines are the best linear fits according to $\rho_H = R_H B$. Curves with negative slope from bottom to top: $T = 4.0, 5.5, 6.3, 7.1, 8.0,$ and 10.0 K. Curves with positive slope from top to bottom: $T = 29.9, 34.9, 39.7, 44.7, 49.7,$ and 54.7 K.

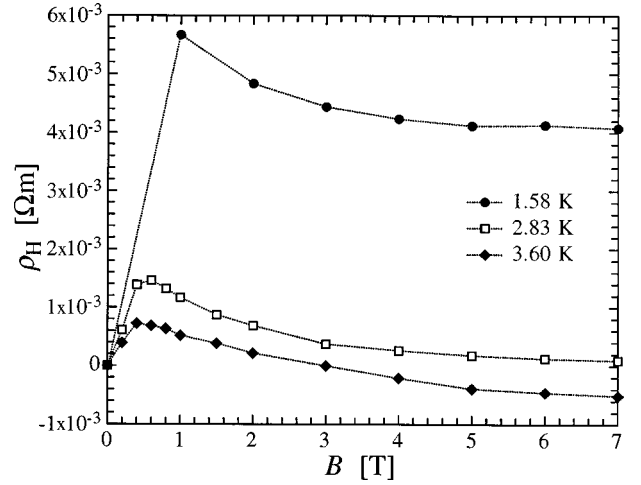


FIG. 4. Some representative Hall resistivity ρ_H vs external magnetic induction $B = \mu_0 H$ isotherms measured on FeSi sample No. 1.

where

$$R_0 = \frac{R_1 \sigma_1^2 + R_2 \sigma_2^2}{\sigma_0^2}, \quad (2)$$

$$R_\infty = \frac{R_1 R_2}{R_1 + R_2}, \quad (3)$$

$$\mu = \frac{\sigma_1 \sigma_2}{\sigma_0} (R_1 + R_2), \quad (4)$$

$$\sigma_0 = \sigma_1 + \sigma_2. \quad (5)$$

Here σ_i and R_i are the conductivity and the Hall coefficient of the i th band ($i = 1, \text{ and } 2$), and R_0 and R_∞ are the Hall coefficients at zero and infinite B , respectively. Both σ_i and R_i are assumed to be independent of B in this model, i.e., single-band effects are neglected.

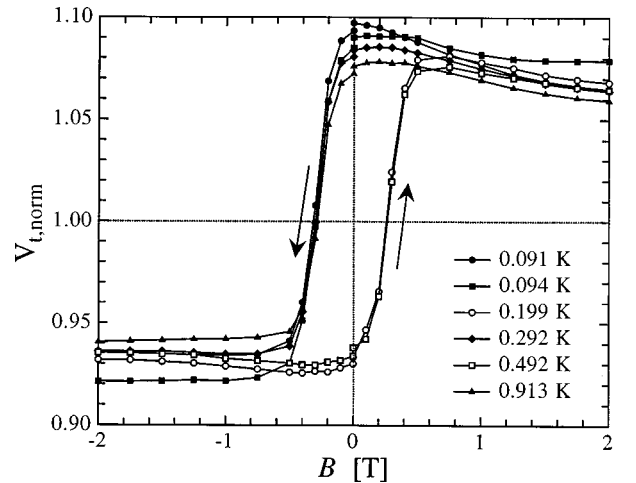


FIG. 5. Transverse voltage V_t normalized to $[V_t(+2T) + V_t(-2T)]/2$ vs external magnetic induction $B = \mu_0 H$ at different fixed temperatures below 1 K measured on FeSi sample No. 1. The arrows indicate the direction in which the magnetic field H was varied.

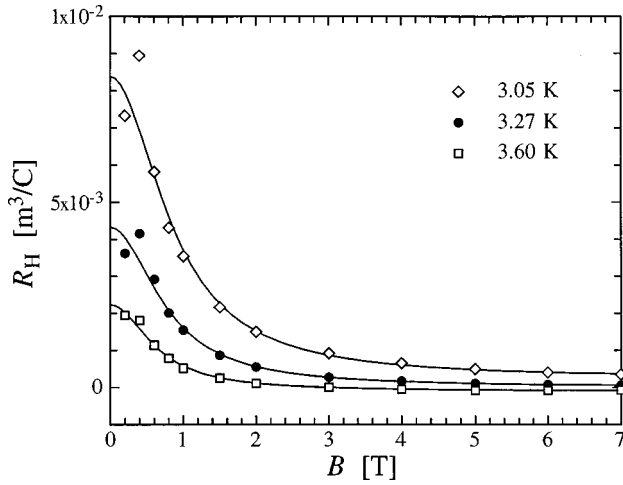


FIG. 6. Some representative isotherms of the Hall coefficient $R_H = \rho_H/B$ as a function of the external magnetic induction $B = \mu_0 H$ of FeSi sample No. 1. The curves are best fits of the presented data to Eq. (1).

Some representative $R_H(B)$ curves together with the fits of Eq. (1) are shown in Fig. 6. Using Eqs. (2)–(5) and inserting the obtained fit parameters R_0 , R_∞ , and μ , as well as the measured zero-field conductivity σ_0 from Fig. 1, we calculated the zero-field conductivities σ_i , the Hall mobilities μ_i , and the Hall coefficients R_i of both sets of charge carriers. We find that $\sigma_2 \ll \sigma_1 \approx \sigma_0$, $\mu_1 \ll \mu_2 \approx 1 \text{ m}^2 \text{ V}^{-1} \text{ s}^{-1}$, and $|R_1| \ll R_2 \approx 100 \text{ m}^3 \text{ C}^{-1}$, corresponding to approximately 10^{17} m^{-3} (positive) charge carriers. The total conductivity σ_0 is dictated by band 1 because its higher charge-carrier concentration overcompensates for its lower mobility. Within this two-band analysis the appearance of a hysteresis in the Hall effect below 1 K remains unexplained. It indicates, instead, that magnetic moments are involved, causing a contribution related to the anomalous Hall contribution.

The anomalous Hall effect arises from the spin-orbit coupling between localized moments and itinerant electrons which produces an extra electric field with the same orientation as that induced by the Lorentz force in the normal Hall effect. The Hall resistivity of such a material can be written as^{32,33}

$$\rho_H(B) = R_0 B + R_s \mu_0 M(B), \quad (6)$$

where R_0 and R_s are the normal and spontaneous Hall coefficients, respectively, μ_0 is the vacuum permeability, and M the sample's volume magnetization.

In Fig. 7 we show several isothermal field dependences between 1.9 and 11 K of the magnetization $M(B)$ of the sample that was used for the Hall effect measurements. All $M(B)$ curves were measured by first increasing and then decreasing B . The curves are completely reversible. Fitting the $\rho_H(B)$ data to Eq. 6 by using the experimental values of $M(B)$ gives, at best, only approximate agreement, as may be seen in Fig. 8. The ratio $(R_s \mu_0 M)/(R_0 B)$ in low B fields, a measure of the importance of the anomalous Hall effect, increases only slightly from approximately 1 at 8 K to approximately 2 at 2 K. Values of $(R_s \mu_0 M)/(R_0 B)$ of the order of 1 are between values typical for ferromagnetic semiconductors ($\ll 1$) and values typical for ferromagnetic metals

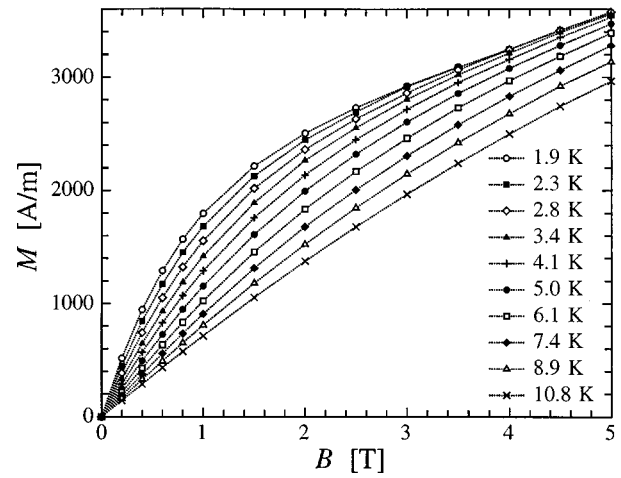


FIG. 7. Magnetization M of FeSi sample No. 1 as a function of the external magnetic induction B at different fixed temperatures. The curves are a guide to the eye.

(> 100).³⁴ The normal Hall coefficient R_0 is negative, over the entire temperature range from 1 to 8 K. The corresponding charge-carrier density varies between 10^{21} and 10^{22} m^{-3} below 4 K, and increases to approximately $5 \times 10^{22} \text{ m}^{-3}$ at 8 K, which is slightly smaller than what is found from linear fits to $\rho_H(B)$ (cf. Fig. 3). The Hall mobility is between 10^{-3} and $10^{-2} \text{ m}^2 \text{ V}^{-1} \text{ s}^{-1}$.

In the absence of magnetization data below 1.9 K we estimated the charge-carrier density in this temperature regime from the slopes of the $\rho_H(B)$ curves at $B > 1.25 \text{ T}$. This is a valid procedure provided that, at these temperatures, $M(B)$ tends to saturate to a constant value at moderate fields. For all temperatures (cf. Fig. 5), we find negative slopes consistent with an electron density of approximately $2 \times 10^{22} \text{ m}^{-3}$.

B. Specific heat

The temperature dependence of the specific heat is presented in Fig. 9 on a double-logarithmic diagram. Except

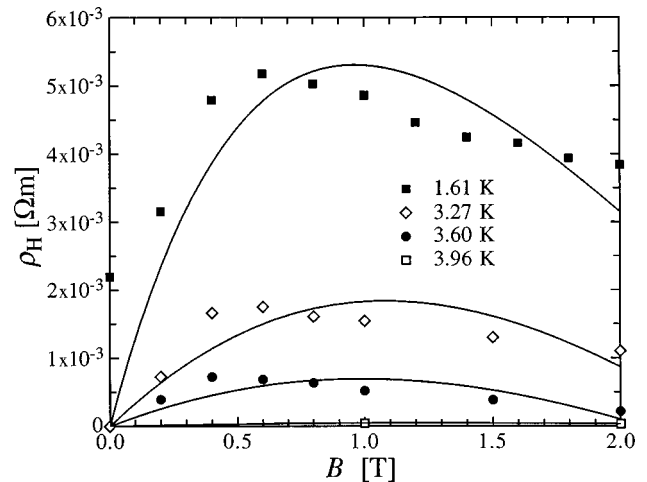


FIG. 8. Selected isotherms of the Hall resistivity ρ_H vs external magnetic induction $B = \mu_0 H$ of FeSi sample No. 1. The curves are best fits according to Eq. (6). For each temperature, an interpolation between the experimental $M(B)$ curves of Fig. 7 was used.

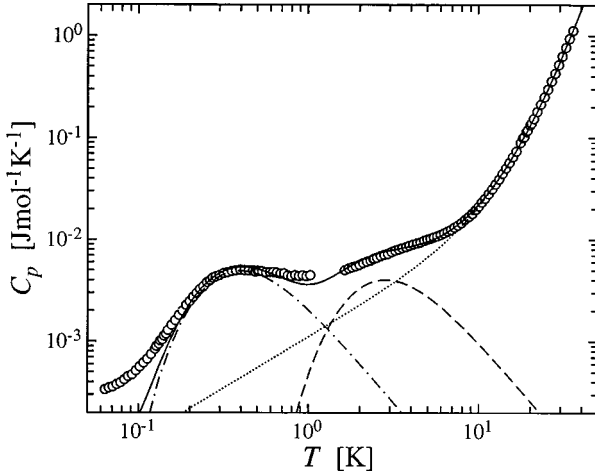


FIG. 9. Temperature variation of the specific heat C_p of FeSi sample No. 2. The solid curve is a best fit to the experimental data according to Eq. (7). The dotted curve corresponds to the contribution of the $\gamma T + \beta T^3 + \delta T^5$ term, the dashed curve to Schottky anomaly 1, and the dash-dotted curve to Schottky anomaly 2.

below 0.2 K, it can reasonably well be described by the sum of the common low-temperature electronic and lattice contributions and two Schottky anomalies resulting from excitations within two different two-level systems with interlevel energy separations of $k_B T_1$ and $k_B T_2$, respectively, i.e.,

$$C_p = \gamma T + \beta T^3 + \delta T^5 + a_1 \frac{(T_1/T)^2 \exp T_1/T}{(1 + \exp T_1/T)^2} + a_2 \frac{(T_2/T)^2 \exp T_2/T}{(1 + \exp T_2/T)^2}. \quad (7)$$

The fit according to this relation is shown as a solid curve in Fig. 9. The fit parameters are $\gamma = 1.1 \times 10^{-3} \text{ J mol}^{-1} \text{ K}^{-2}$, $\beta = 9.1 \times 10^{-6} \text{ J mol}^{-1} \text{ K}^{-4}$, $\delta = 1.1 \times 10^{-8} \text{ J mol}^{-1} \text{ K}^{-6}$, $a_1 = 9.2 \times 10^{-3} \text{ J mol}^{-1} \text{ K}^{-1}$, $T_1 = 6.8 \text{ K}$, $a_2 = 1.1 \times 10^{-2} \text{ J mol}^{-1} \text{ K}^{-1}$, and $T_2 = 0.95 \text{ K}$. From the low-temperature lattice contribution βT^3 , we calculate a Debye temperature $\Theta_D = 377 \text{ K}$ distinctly higher than the Debye temperature $\Theta_D = 314 \text{ K}$ calculated from the the elastic constants c_{11} and c_{44} measured at room temperature.³⁵ The entropy releases corresponding to the Schottky anomalies are $\Delta S_1 = 6.3 \text{ mJ mol}^{-1} \text{ K}^{-1}$ and $\Delta S_2 = 7.9 \text{ mJ mol}^{-1} \text{ K}^{-1}$, i.e., approximately 0.11% and 0.14% two-level centers per FeSi unit, respectively. Possible reasons for the excess specific heat below 0.2 K are discussed below.

C. Magnetic susceptibility

In Fig. 10 the temperature dependence of the magnetic susceptibility χ is shown on a double-logarithmic plot. As previously established, χ decreases from 330 to 90 K, and rises again at lower temperatures. Our high-temperature ($T > 90 \text{ K}$) susceptibility data compare well with published $\chi(T)$ data on both poly-crystalline and single-crystalline FeSi.^{2,4,9,19–21,36} A good description of $\chi(T)$ over the whole temperature range is obtained by the sum of a thermally activated contribution and two Curie-Weiss-type contributions, i.e.,

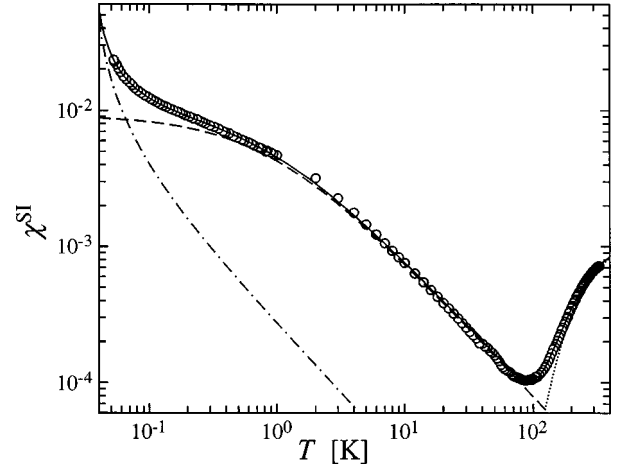


FIG. 10. Temperature variation of the magnetic susceptibility χ of FeSi sample No. 2. The fit according to Eq. (8) is shown as the solid curve. The dotted, dashed, and dash-dotted curves correspond to the first, second, and third term of Eq. (8), respectively.

$$\chi = \frac{c}{T} \exp(-T_0/T) + \frac{C_1}{T - \Theta_1} + \frac{C_2}{T - \Theta_2}. \quad (8)$$

The fit is shown in Fig. 10 as a solid curve. The fit parameters are $c = 1.8 \text{ K}$, $T_0 = 670 \text{ K}$, $C_1 = 8.0 \text{ mK}$, $\Theta_1 = -870 \text{ mK}$, $C_2 = 0.26 \text{ mK}$, and $\Theta_2 = +34 \text{ mK}$. The first Curie-Weiss term with a negative value of Θ is consistent with predominantly antiferromagnetically coupled moments of $0.26 \mu_B/\text{FeSi}$ unit, and the second Curie-Weiss term with a positive value of Θ is consistent with predominantly ferromagnetically coupled moments of $0.05 \mu_B/\text{FeSi}$ unit. Most likely the moments arise from uncompensated iron. Assuming that due to the low symmetry (C_3) of the Fe sites in FeSi, the angular momentum of the Fe ions is quenched, i.e., $L=0$ and $J=S$, and that the Fe moments may be considered as noninteracting with their environment, i.e., $g_J=2$, the configurations $d^7\text{Fe}^+$, $d^6\text{Fe}^{2+}$, and $d^5\text{Fe}^{3+}$ lead to the ionic magnetic moments of $3.9 \mu_B$, $4.9 \mu_B$, and $5.9 \mu_B$, respectively. For $d^7\text{Fe}^+$, for example, C_1 thus corresponds to a moment density of $2.04 \times 10^{26} \text{ m}^{-3}$ and C_2 to $6.75 \times 10^{24} \text{ m}^{-3}$.

D. Optical reflectivity

Figure 11 presents the reflectivity R and the optical conductivity σ_1 for some significant temperatures. As described below, the overall temperature dependence and the most prominent absorptions are in agreement with our previous investigation of a single crystal grown in antimony flux,²⁴ and of a polycrystalline specimen of pure FeSi.³⁷ Our results are similar to those obtained by other groups.^{9,38–40} The most striking feature is the strong temperature dependence of $R(\omega)$ in the FIR spectral range, where the reflectivity changes from a metallic behavior at temperatures above 100 K by tending toward 100% for $\omega \rightarrow 0$, to that of an insulator below 40 K. This can also easily be recognized on plots of the optical conductivity $\sigma_1(\omega)$. As the temperature decreases, the low-frequency limit of $\sigma_1(\omega)$ drops continuously and, below 40 K, it is vanishing small, typical of insulators. Figure 11(b) reveals that the Drude component of

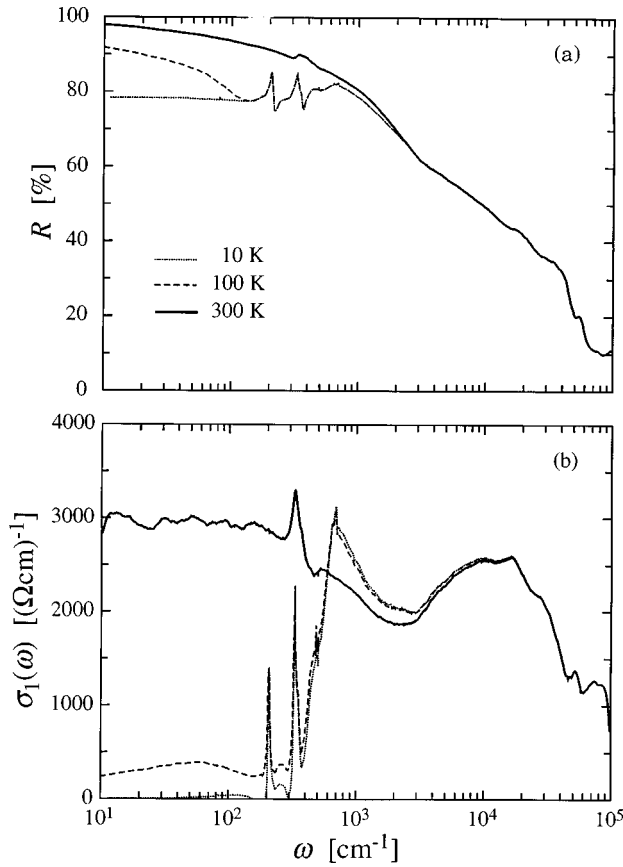


FIG. 11. Optical reflectivity $R(\omega)$ (a) and optical conductivity $\sigma_1(\omega)$ (b) of FeSi sample No. 2 at 300, 100 and 10 K.

$\sigma_1(\omega)$ ascribed to itinerant charge carriers is progressively quenched down to 100 K, and disappears below 40 K. Several distinct and narrow modes appear in the FIR frequency range upon decreasing the temperature to 10 K. We also note that the electrodynamic response of $\text{Fe}_{1-x}\text{Co}_x\text{Si}$ with $x \leq 0.03$ is qualitatively and quantitatively similar to that of pure FeSi, except in the FIR range, where the increasing metallicity for $x \geq 0.01$ is evidenced by an increasing amplitude of the low-temperature Drude component.³⁷

IV. DISCUSSION

A. High-temperature properties

1. Magnetic susceptibility

First we shall focus on the magnetic susceptibility between 100 and 330 K. Jaccarino *et al.*² noted that their high-temperature magnetic susceptibility data can be described in two different ways: either by considering a system of free ions with spin zero in their ground state and spin S in their excited state, or by invoking metallic spin paramagnetism in two extremely narrow bands separated by a small energy gap.

The “free-ion-like” model provides the equation

$$\chi = \frac{Ng^2\mu_B^2\mu_0}{3k_B T} \frac{S(S+1)(2S+1)}{2S+1 + \exp(-T_0/T)}. \quad (9)$$

The first term in Eq. (8), i.e., $c/T \exp(-T_0/T)$, which accounts for the high-temperature contribution to $\chi(T)$ can, in

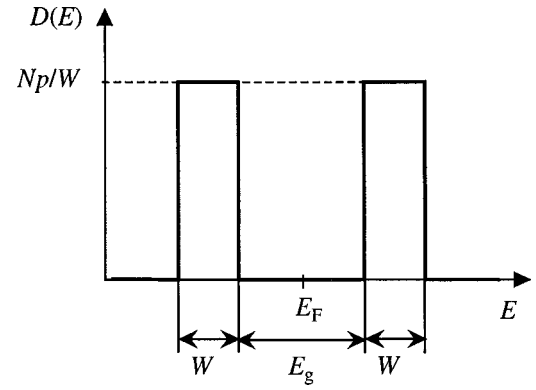


FIG. 12. Model density of states first proposed by Jaccarino *et al.* (Ref. 2) to fit the high-temperature $\chi(T)$ data of FeSi within a “metallic-paramagnetism” model.

fact, be considered as an approximation of Eq. (9) for $T \ll T_0$. If we replace the first term of Eq. (8) by Eq. (9), and also allow, in the fitting procedure, the parameters of the Curie-Weiss terms to readjust, we find a satisfactory agreement between calculation and experiment only with $S=1$. With the g factor fixed to 2 and with $N=4/a^3=4.42 \times 10^{22} \text{ cm}^{-3}$ for the density of Fe ions, $T_0=740 \text{ K}$ (64 meV) and the parameters of the two Curie-Weiss terms remain essentially unchanged from those obtained by fitting with Eq. (8). For $S=\frac{1}{2}$ and $\frac{3}{2}$, no fit of equal quality can be obtained with the g factor fixed to 2. Jaccarino *et al.*² reported the best agreement for $S=\frac{1}{2}$, where $g=3.92$ and $T_0=750 \text{ K}$, and a somewhat poorer agreement for $S=1$ with $g=2.17$ and $T_0=795 \text{ K}$. Since the physical origin of a strongly enhanced g factor within this simple two-level model is not clear, we tend to favor the $S=1$ interpretation in this case.

The model DOS which Jaccarino *et al.*² used in the “metallic-paramagnetism” model is depicted in Fig. 12. Two rectangular peaks of width W and height $D(E) = pN/W$, separated by an energy gap of width E_g , are introduced to approximate the DOS of FeSi in the vicinity of the Fermi level. N is the density of unit cells containing four FeSi units, and p is the total number of states per unit cell. The Fermi energy E_F is situated in the middle of the gap. The Pauli susceptibility of this system is readily calculated from

$$\chi^{\text{Pauli}}(T) = -2\mu_0\mu_B^2 \int_{\text{conduction band}} D(E) \frac{\partial f(E, E_F, T)}{\partial E} dE, \quad (10)$$

where $f(E, E_F, T)$ is the Fermi function. The factor 2 accounts for the fact that holes in the valence band contribute to χ in the same way as electrons in the conduction band. For χ^{Pauli} to vanish as $T \rightarrow 0$, the number of electrons per Fe atom has to be an even number. Jaccarino *et al.*² reported good agreement of this expression with their $\chi(T)$ data only in the limit $W \ll E_g$. They fixed the number of electrons to two per Fe atom, i.e., in our notation $p=8$. More recently other authors^{21,41} employed the same model DOS and reported good agreement with a non-negligible bandwidth W , in agreement with our results if we fix $p=16$. In fact, the Pauli paramagnetism resulting from two rectangular DOS features is compatible with the $\chi(T)$ data of FeSi, including the data

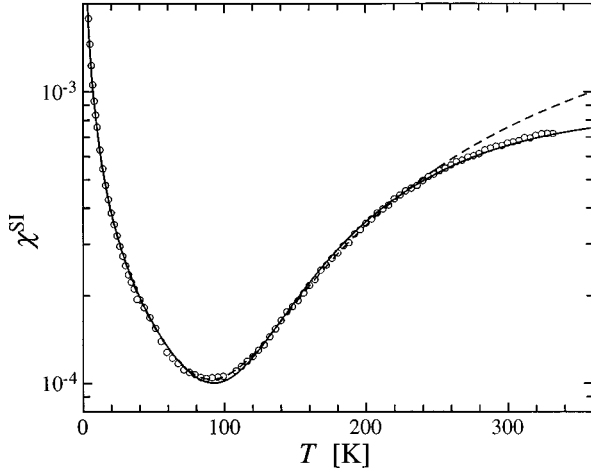


FIG. 13. Temperature dependence of the magnetic susceptibility χ of FeSi sample No. 2. The open circles are the experimental data points. The solid and dashed curves represent the fit Nos. 1 and 2, respectively, of Table I.

above room temperature,^{2,21,36} only if $p=16$, i.e., only if there are four itinerant electrons per Fe site. The fit to our data is shown as a solid curve in Fig. 13 and the fit parameters are given in Table I (fit No. 1). The constant density of states of the two bands is $D(E)=435$ states/unit cell/eV. Band-structure calculations^{13,15-19} predict a peak in the DOS just above the gap of approximately 13 states/unit cell/eV, i.e., more than a factor 30 less.

The model DOS depicted in Fig. 12 captures two important features, namely, that the two peaks on both sides of the energy gap are narrow, and that they have sharp edges. The narrow width of the peaks is only important at very high temperatures, where the lower band (upper band) starts to be considerably depleted (filled), and where the probability of a thermal excitation to energies above the upper band is not negligible. The sharp edges are particularly important at lower temperatures. Here the infinite slope of the rectangular DOS should be replaced by the more physical assumption of parabolic bands with renormalized curvature. Hence we also fitted the $\chi(T)$ data with two parabolic bands, with the density of states in the conduction band,

$$D_c(E) = 2 \frac{1}{(2\pi)^2} \left(\frac{2m_c}{\hbar^2} \right)^{3/2} (E - E_c)^{1/2}, \quad (11)$$

TABLE I. Results of the fits of the $\chi(T)$ data of FeSi sample No. 2 to Eq. (8) with its first term replaced by the high-temperature Pauli susceptibility of Eq. (10). Fit No. 1 uses the model DOS of Fig. 12, i.e., two rectangular DOS peaks described by the parameters T_g , T_w , and p . Fit No. 2 uses two parabolic bands described by the parameters T_g and m_c^* . The temperature range in which the $\chi(T)$ data were fitted is denoted as the T range. The value marked with an asterisk was kept fixed during the fitting procedure. p/W is the DOS of the rectangular peaks.

Fit No.	T range	T_g (K)	T_w (K)	p	p/W (states/eV/cell)	m_c^*
1	<330 K	1130	425	16*	435	
2	<250 K	870				195

and an analogous relation for the density of states in the valence band $D_v(E)$. A high value of m_c (and m_v) leads to a sharply rising DOS near the gap. For simplicity we assumed $m_c = m_v$, so that the Fermi energy lies in the middle of the gap. We further introduce the effective-mass ratios $m_c^* = m_c/m_0$ and $m_v^* = m_v/m_0$, where m_0 is the free-electron mass.

The dashed curve in Fig. 13 is the fit which is obtained if, instead of the rectangular DOS of Fig. 12, two parabolic bands characterized by $m_c^* = m_v^*$ are used. The $\chi(T)$ data were fitted only below 250 K. At higher temperatures the parabolic bands fail to describe the experimental data, as expected from the above-mentioned arguments. The corresponding fit parameters are also given in Table I (fit No. 2). The assumption of different DOS shapes changes the absolute value of the gap, $T_g = 1130$ K (97 meV) for rectangular DOS peaks to $T_g = 870$ K (75 meV) for parabolic bands. For the effective-mass ratio, the second fit yields $m_c^* = 195$. It is not surprising that, except at very high temperatures, parabolic bands with extremely high effective masses give similar results as the rectangular DOS peaks.

The effective mass m_c entering Eq. (11) is a so-called density-of-states effective mass which characterizes the total density of states but not necessarily that of a single valley of the conduction band. In the case where ν conduction-band minima with effective mass m_n occur at symmetrical points of the Brillouin zone⁴²

$$m_c = \nu^{2/3} m_n. \quad (12)$$

Similarly, if two separate bands of mass m_{n1} and m_{n2} are degenerate in energy at their minima,⁴²

$$m_c = (m_{n1}^{3/2} + m_{n2}^{3/2})^{2/3}. \quad (13)$$

Band-structure calculations indicate that this type of consideration is of particular importance in the case of FeSi. Not only do we face high valley degeneracies ν , but we also notice several conduction-band (valence-band) minima (maxima) to occur within a few meV of the gap edge, such that, at high temperatures, they are essentially degenerate. Assuming for each of these minima (maxima) the same effective mass $m_n(m_p)$ we estimate from the band-structure results of Ref. 15 the density-of-states effective masses $m_c = 13m_n$ and $m_v = 21m_p$.

2. Electrical conductivity and Hall effect

Next we analyze the electrical conductivity between approximately 30 and 300 K, which we identify as the temperature range of intrinsic conduction. We have calculated the conductivity using the rectangular DOS model of Fig. 12, which was previously done by Mandrus *et al.*⁴¹ and Sales *et al.*²¹ For simplicity, we first assume the same mobility for the valence and the conduction bands, i.e., $\mu_n = \mu_p = \mu$, and we have

$$\sigma = 2e\mu n \quad \text{with } n = \int_{\text{conduction band}} D(E)f(E) dE. \quad (14)$$

It is clear that fits to the conductivity are more ambiguous than fits to $\chi(T)$, because of the dependence of σ on the

TABLE II. Results of the fits of the $\sigma(T)$ data of FeSi sample No. 1 to Eq. (14). Fit No. 1 uses two rectangular DOS peaks described by the parameters T_g , T_W , and p . Fit No. 2 uses two parabolic bands described by the parameters T_g and m_n^* . The mobility $\mu = aT^{-\alpha}$ introduces the parameters a and α , but in the case of two parabolic bands $m_n^{*3/2}$ and a are not linearly independent, and were therefore fitted together. The temperature range in which the $\sigma(T)$ data were fitted is denoted as T range. The values marked with an asterisk were kept fixed during the fitting procedure.

Fit No.	T range	T_g (K)	T_W (K)	p	a ($\text{m}^2 \text{K}^\alpha \text{V}^{-1} \text{s}^{-1}$)	α	$am_n^{*3/2}$ ($\text{m}^2 \text{K}^\alpha \text{V}^{-1} \text{s}^{-1}$)
1	> 100 K	785	425*	16*	0.45	1.5*	
2	$50 \text{ K} < T < 140$ K	650				1.5*	1940

mobility. A reasonable first choice for the temperature dependence of μ is a power-law dependence $\mu = aT^{-\alpha}$ which introduces two additional parameters. We obtain a very good fit with $T_g = 815$ K, $\alpha = 1.59$, $a = 0.77 \text{ m}^2 \text{K}^{3/2} \text{V}^{-1} \text{s}^{-1}$, and $T_W = 425$ K, which was fixed to the value obtained in our $\chi(T)$ fit (fit No. 1 of Table I). An equally good fit, shown as a solid curve in Fig. 14, is obtained if in addition we fix $\alpha = 1.5$ (fit No. 1 of Table II), which is the exponent of acoustic-phonon scattering also introduced in the calculations of Refs. 21, 37, and 41. On the other hand, no satisfactory agreement can be obtained if we fix the gap width to the value $T_g = 1130$ K obtained in our $\chi(T)$ fit (fit No. 1 of Table I). This suggests that, within the same model, the gap relevant for the conductivity is smaller than the gap relevant for the susceptibility.

We also fitted the $\sigma(T)$ data with two parabolic bands and their density of states in the conduction band represented by Eq. (11). The result is shown as a dashed curve in Fig. 14 and the parameters are given in Table II (fit No. 2). As for $\chi(T)$, assuming parabolic bands again fails to describe the experimental data at the highest temperatures. Fixing T_g to the value obtained for the $\chi(T)$ fit with parabolic bands (fit No. 2 of Table I) gives unsatisfactory agreement with the data, indicating that the energy gaps effective for χ and σ are again not the same, thus supporting the conclusion from the comparison of the $\chi(T)$ and $\sigma(T)$ fits using two rectangular DOS peaks mentioned above. Possible explanations are that either the smallest gap is an indirect gap relevant for σ but

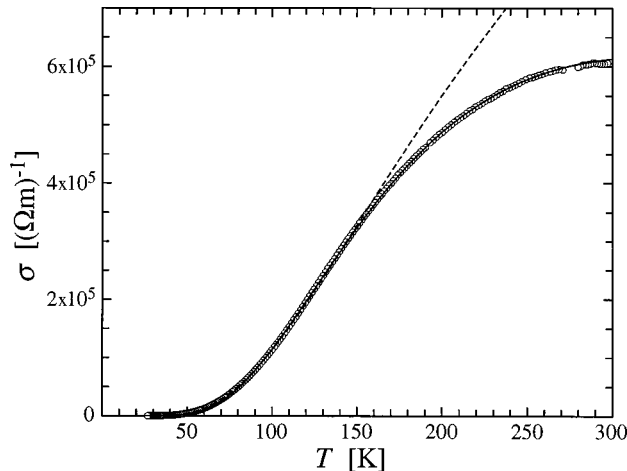


FIG. 14. Temperature dependence of the conductivity σ of FeSi sample No. 1. The open circles are the experimental data points. The solid and dashed curves represent the fit Nos. 1 and 2, respectively, of Table II.

not for χ , as is predicted by band-structure calculations,^{15–17} or that we have spin and charge gaps of different width. As we will show below, our optical data favor the first explanation.

For a description of the conductivity consistent also with our Hall-effect measurements, we have to drop the restriction of equal mobilities μ_n and μ_p adopted in Eq. (14), this in order to account for the nonvanishing Hall coefficient in the intrinsic regime. In Fig. 15 we present the conductivity $\sigma(T)$ and the itinerant charge carrier concentration $n(T)$

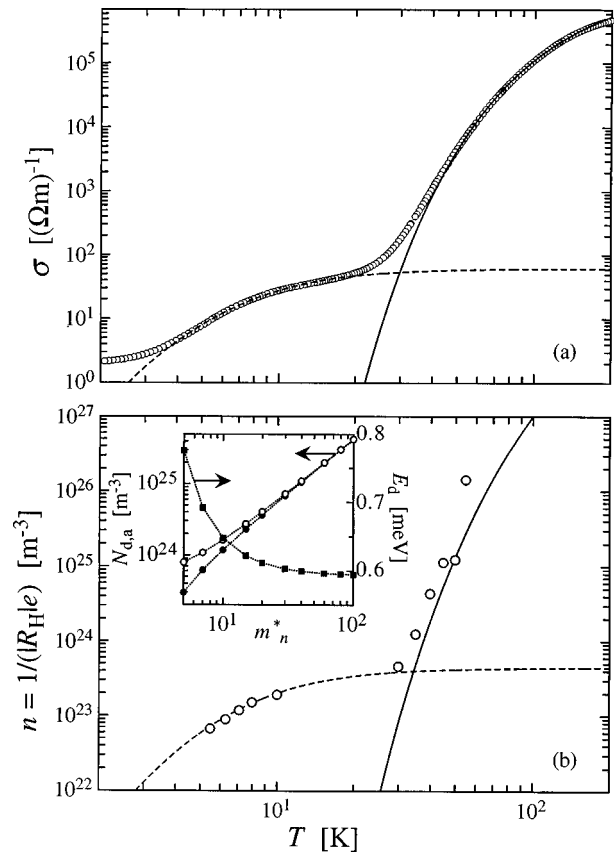


FIG. 15. Double-logarithmic plots of (a) the electrical conductivity σ and of (b) the charge carrier concentration $n = 1/(|R_H|e)$ taken from Fig. 3, both measured on FeSi sample No. 1. R_H is positive at $T > 20$ K and negative at $T < 10$ K. The solid and dashed curves represent the fits explained in the text. The inset shows the result of fits of Eq. (20) to the $\sigma(T)$ data in the extrinsic regime. The donor and acceptor concentrations N_d and N_a , shown as open and full circles, respectively, and the donor energy E_d are given as a function of the effective-mass ratio of the conduction band $m_n^* = m_n/m_0$, which was kept fixed during each fit.

$=1/(|R_H|e)$ (taken from Fig. 3) on double-logarithmic plots. The overall behavior of $\sigma(T)$ and $n(T)$ is quite similar, which indicates that the temperature dependence of σ is essentially due to the temperature dependence of the charge-carrier concentration, the temperature dependence of the mobility playing a minor role. The conductivity and the inverse Hall coefficient of an intrinsic semiconductor are⁴³

$$\sigma_{\text{in}} = e(\mu_n + \mu_p)n_{\text{in}} \quad (15)$$

and

$$\frac{1}{R_{H_{\text{in}}}} = e \frac{1}{r_H} \frac{\mu_n + \mu_p}{\mu_p - \mu_n} n_{\text{in}} \quad (16)$$

with

$$n_{\text{in}} = 2m_n^{*3/2} \left(\frac{m_0 k_B T}{2\pi\hbar^2} \right)^{3/2} \mathcal{F}_{1/2} \left(-\frac{E_g}{2k_B T} \right). \quad (17)$$

$\mathcal{F}_{1/2}(x)$ is the Fermi-Dirac integral of order $\frac{1}{2}$, which approaches for $x \ll 0$ the classical value $\exp(x)$. Assuming $\mu_{n,p} = a_{n,p} T^{-\alpha}$ and for the Hall factor $r_H = 1$, we obtain

$$\frac{\sigma_{\text{in}}}{1/R_{H_{\text{in}}}} = (a_p - a_n) T^{-\alpha}. \quad (18)$$

A good fit of Eq. (18) to the data between 30 and 55 K with $\alpha = 1.5$ is possible, and yields $a_p - a_n = 0.38 \text{ m}^2 \text{ K}^{3/2} \text{ V}^{-1} \text{ s}^{-1}$. For $\sigma(T)$ we use the fit that was shown as a dashed curve in Fig. 14, and that we replotted as a solid curve in Fig. 15(a). The fit parameters are $E_g = 56 \text{ meV}$ and, since now $\mu = (\mu_n + \mu_p)/2$, $m_n^{*3/2}(a_n + a_p)/2 = 1940 \text{ m}^2 \text{ K}^{3/2} \text{ V}^{-1} \text{ s}^{-1}$ (fit No. 2 of Table II). Using these results and Eq. (16), we calculate $n(T) = 1/(|R_H|e)$, which is shown as a solid curve in Fig. 15(b).

3. Reflectivity and optical conductivity

The most relevant feature of the electrodynamic response of FeSi is the MIR absorption at 770 cm^{-1} (95 meV), which is associated with a semiconductor-type gap.⁹ Band-structure calculations^{15–17} predict a value for the direct gap of 140 meV, only in an order-of-magnitude agreement with experiment. The gap value derived from our optical data compares relatively well with the gap value extracted from fits of $\chi(T)$ to the “metallic-paramagnetism” model described above (97 meV for rectangular DOS peaks, 75 meV for parabolic bands), but is considerably larger than the gap energy extracted from fits of $\sigma(T)$ to the same model (68 and 56 meV for rectangular DOS peaks and for parabolic bands, respectively). This is an indication that the smallest gap relevant for transport measurements is an indirect gap, and that the direct gap has the same width for both charge and spin excitations, in agreement with the findings of Sales *et al.*²¹ and Mihalik

*et al.*²² For polycrystalline FeSi, the difference of the energy-gap values extracted from optics and from $\sigma(T)$ is much less pronounced.³⁷

An important issue concerns the redistribution of the missing spectral weight below the gap. In our data, that spectral weight is essentially recovered at a frequency $\omega_c \approx 4\omega_g$, where $\omega_g = 770 \text{ cm}^{-1}$ is the gap excitation frequency, i.e., there is no need for an integration of $\sigma_1(\omega)$ to very high frequencies in order to satisfy the spectral-weight sum rule. In our previous optical investigation²⁴ of an FeSi single crystal grown in antimony flux, the same conclusion was offered. However, the redistribution of the spectral weight still remains a controversial experimental issue. In fact, our conclusion is at variance with claims based on previously reported optical results on FeSi.⁹ Recent Raman-scattering studies of FeSi (Ref. 44) reveal an abrupt suppression of low-frequency electronic Raman scattering below $T < 250 \text{ K}$. Even though this might be more consistent with correlation-gap models than with a conventional band-gap description, the electronic spectral weight which is lost at low frequencies because of the charge gap, is primarily recovered within the energy range $\omega < 3\omega_g$.^{24,44}

In the high-frequency spectral range above the gap, we recognize a broad absorption at about 1 eV, and two less intensive ones at approximately 6 and 10 eV. There is a good agreement with the spectra of Ref. 38, where the measurements were extended up to 30 eV. The absorption at 6 and 10 eV is ascribed to electronic interband transitions, in rather good agreement with band-structure calculations.^{15,16} The feature at about 1 eV is incompatible with the band-structure calculations, and was suggested to be induced by strong spin correlations.³⁸

B. Intermediate-temperature properties

Here we focus on the properties at temperatures between approximately 4 and 30 K, which turn out to be dominated by defects. We start with an analysis of the conductivity and the Hall-effect data. As shown in Fig. 15, the $\sigma(T)$ and $n(T) = 1/(|R_H|e)$ data below approximately 30 K cannot be accounted for with a band structure of an intrinsic semiconductor (e.g., two parabolic bands) and one has to assume the presence of donors and/or acceptors. The σ and R_H data in this so-called extrinsic regime can be well described using a simple model for a partially compensated n -type semiconductor. Donor levels with a concentration N_d are situated at an energy E_d below the conduction-band edge E_c , and acceptor levels with a concentration N_a lie well below the Fermi level E_F , but at otherwise arbitrary energy. Additional donor states which lie well below E_F are allowed, but will have no bearing on the solution of the problem since they all retain their electrons. This situation was analyzed in detail in Ref. 42, for the case of parabolic conduction and valence bands. In the case $E_F - E_c \leq 1.3 k_B T$, an analytical solution of the problem is possible, and yields, for the carrier concentration in the conduction band,

$$n_{\text{ex}} = \frac{2N_c N_{\text{diff}}}{N_c + CN_{\text{diff}} + \frac{N_a \exp E_d}{k_B T} + \sqrt{\left[N_c - CN_{\text{diff}} + \frac{N_a \exp E_d}{k_B T} \right]^2 + \frac{4(N_c + CN_a)N_{\text{diff}} \exp E_d}{k_B T}}}$$

with

$$N_{\text{diff}} = N_d - N_a, \quad N_c = 2 \left(\frac{m_n k_B T}{2 \pi \hbar^2} \right)^{3/2}, \quad C = 0.27. \quad (19)$$

In the extrinsic regime,

$$\sigma_{\text{ex}} = e \mu_n n_{\text{ex}} \quad (20)$$

and

$$\frac{1}{R_{H_{\text{ex}}}} = e \frac{1}{r_H} n_{\text{ex}}. \quad (21)$$

Using $r_H = 1$, as above, this leads to $\sigma_{\text{ex}}/(1/R_H)_{\text{ex}} = \mu_n$. The measured values of $\sigma/(1/R_H)$ are roughly constant in the extrinsic temperature regime, and a corresponding fit yields $\mu_n = 8.6 \times 10^{-4} \text{ m}^2 \text{ V}^{-1} \text{ s}^{-1}$. The fit of Eq. (20) to the $\sigma(T)$ data between 4 and 16 K, shown as a dashed curve in Fig. 15(a), does not allow us to determine all fit parameters N_d , N_a , E_d , and m_n in a unique way. Therefore, we fixed m_n in the fitting procedure, and determined N_d , N_a , and E_d as functions of m_n . The results are shown in the inset of Fig. 15. With decreasing $m_n^* = m_n/m_0$, E_d increases slightly, and we go over from a strongly to a less compensated n -type semiconductor. The carrier concentration $n = 1/(|R_H|e)$, calculated from the $\sigma(T)$ fit and the value of μ_n given above, is shown as a dashed curve in Fig. 15(b).

As has been elaborated in Sec. IV A 1, m_n is the effective mass relevant for the conductivity, because in a semiconductor with valley degeneracy ν the conductivity effective mass is equal to the effective mass associated with a single valley. According to our discussion of the density-of-states effective-mass ratio $m_c^* = 195$ in Sec. IV A 1, we would expect a conductivity effective-mass ratio m_n^* of the order of 10, as will be confirmed by some cross-checks to be outlined below.

If we associate the donor states at the energy E_d below the conduction-band edge with impurity states in a semiconductor, their energy may be calculated within the simple hydrogen model

$$E_d = \frac{m_n^*}{\epsilon_{\text{eff}}} \times 13.6 \text{ eV}. \quad (22)$$

The relevant dielectric constant ϵ_{eff} is the static dielectric constant $\epsilon_0 = \epsilon_1(\omega \rightarrow 0)$, which we determined from our optical data to be 380. From $E_d(m_n^*)$ in the inset of Fig. 15, and Eq. (22), we obtain $m_n^* = 7.3$ and $E_d = 0.69 \text{ meV}$. With this effective-mass ratio we further find $N_d = 1 \times 10^{24} \text{ m}^{-3}$, and $N_a = 7 \times 10^{23} \text{ m}^{-3}$. Likewise we may now calculate the mobilities in the intrinsic range $\mu_n \lesssim \mu_p = 100(T[K])^{-3/2} \text{ m}^2 \text{ V}^{-1} \text{ s}^{-1}$. The concentration $N_d = 1 \times 10^{24} \text{ m}^{-3}$ corresponds to approximately one donor per 4×10^4 FeSi units, or 25 ppm. Such a low concentration of defects could easily result from local fluctuations in the relative concentrations of Fe and Si in FeSi or from a slight Si deficiency.

Further evidence of electronic states at a small energy E_d of the order of 1 meV or less below the conduction-band edge is provided by the experimental data of the specific heat, the magnetic susceptibility, and the optical reflectivity.

The Schottky anomaly of $C_p(T)$ with a maximum at approximately 3 K shown in Fig. 9, which is compatible with excitations within two-level states of the concentration $4.8 \times 10^{25} \text{ m}^{-3}$ separated by $k_B T_1 = 0.59 \text{ meV}$, may be identified as excitations between the donor states and the conduction band. The interlevel separation $k_B T_1$ agrees reasonably well with the donor binding energy $E_d = 0.69 \text{ meV}$, and the two-level state density with the donor density $N_d = 1 \times 10^{24} \text{ m}^{-3}$ found for $m_n^* = 7.3$, particularly in view of the relatively crude approximations made in the analysis of both C_p and of σ and n . Even so, we would like to mention that a better agreement can be obtained by assuming a higher effective-mass ratio, e.g., $m_n^* = 100$, corresponding to $E_d = 0.59 \text{ meV}$ and $N_d = 4.3 \times 10^{25} \text{ m}^{-3}$. In all, it seems justified to associate this Schottky anomaly with electronic excitations from energetically well-defined donor states into the conduction band.

The temperature dependence of the magnetic susceptibility at intermediate temperatures may also be described by invoking the doped-semiconductor scenario. The moment densities compatible with the Curie-Weiss-type contribution in this temperature range are higher than the donor and acceptor densities discussed above, which can be explained as follows. If we assume that, depending on coordination, Fe defects with different ionization states exist, we may expect that only those defects with energies close to the conduction-band (valence-band) edge act as donors (acceptors), but that all ionized Fe defects in different ionization configurations contribute to the Curie-Weiss-type behavior. If Fe acts as a donor, another estimate of the effective mass can be made by replacing the 13.6 eV in Eq. (22) by the ionization energy of free Fe, $E_I = 7.87 \text{ eV}$ which, together with the inset of Fig. 15 results in $m_n^* = 12$, $E_d = 0.64 \text{ meV}$, $N_d = 2.0 \times 10^{24} \text{ m}^{-3}$, and $N_a = 1.6 \times 10^{24} \text{ m}^{-3}$.

In a previous optical investigation²⁴ of an FeSi single crystal grown in antimony flux evidence of a broad maximum of $\sigma_1(\omega)$ in the spectral range around 10 cm^{-1} ($\approx 1 \text{ meV}$) was found, a feature that could be associated with the optical excitation of electrons from donor levels at E_d into the conduction band.

We thus have a good deal of evidence of a conductivity effective-mass ratio of the order of 10 rather than of the order of 1, as predicted by band-structure calculations. From the band structure given by Mattheiss and Hamann,¹⁵ we extracted, by using crude parabolic fits in narrow regions around the valence-band maximum along the ΓR line and the conduction-band minimum along the ΓM line, the ratios $m_n^* \approx 1.7$ and $m_p^* \approx 0.7$.

The electron mobility μ_n in the extrinsic regime of the order of $10 \text{ cm}^2 \text{ V}^{-1} \text{ s}^{-1}$, is extremely low, two orders of magnitude lower than in doped Ge at the same donor concentration. In the following we show that further evidence of the charge carriers having low mobilities in this temperature range is indicated by our magnetoresistance data.

As was shown in Fig. 2, the magnetoresistance MR at 7 T is negative between 0.05 and 30 K, an indication of the importance of quantum interference effects, which are the crucial process leading to weak localization in weakly disordered electronic systems. Our $\sigma(T)$ data give no additional indications for weak localization. The strong temperature de-

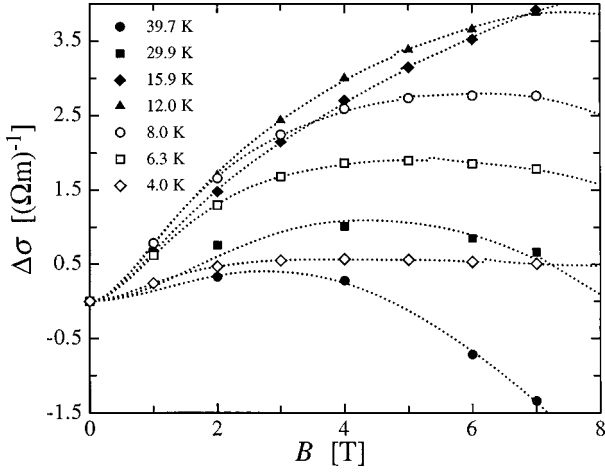


FIG. 16. Magnetoconductivity $\Delta\sigma = \sigma(B) - \sigma(B=0)$ of FeSi sample No. 1 as a function of the external magnetic induction $B = \mu_0 H$ at different temperatures. The curves are fits according to the model described in the text.

pendence of σ due to the variation of the charge carrier concentration probably overshadows the small expected corrections in $\sigma(T)$. The expression for the magnetoresistance in the case of weak localization^{45–47} involves an inelastic relaxation time τ_i and a relaxation time for the spin-orbit scattering τ_{so} as parameters. A second important contribution to the magnetoresistance in weakly disordered systems is the interaction between electrons. An attractive interaction leads to a negative contribution to MR, a repulsive interaction to a positive one. The magnetoresistance in case of interactions^{45,48} consists of an orbital part containing the interaction constant $g(B, T, E_F)$ and of a spin part containing the screening parameter for the Coulomb interaction F . In addition, the diffusion constant D enters as a fit parameter. We used analytic expressions of the relevant formulae^{49,50} to fit our data. Since all the magnetic field corrections $\Delta\rho/\rho$ to the resistivity are proportional to the zero-field resistivity ρ itself, it is adequate to fit $\Delta\sigma = -\Delta\rho/\rho^2$. Some representative $\Delta\sigma(B)$ curves at temperatures between 4 and 40 K are shown in Fig. 16, together with the obtained fits. The contributions of weak localization and of the orbital part of the electron-electron interaction have to be taken into account to obtain good agreement. In Table III we give the obtained fit parameters at several temperatures. The order of magnitude of these values seems to be reasonable. Since we do not have to do with a simple single-band metal but with a doped semiconductor, the situation is very complex, and a more detailed analysis of these results is beyond the scope of this paper.

C. Low-temperature properties

Finally we discuss our experimental results for FeSi at very low temperatures. The interpretation of the conductivity

TABLE III. Parameters of the fits of $\Delta\sigma(B)$ at different temperatures.

T (K)	D (cm ² /s)	τ_i (ps)	τ_{so} (ps)	T_F (K)
40	15	0.1	0.5	4×10^4
10	6.5	0.3	3.3	1.3×10^4
5	2.5	0.5		0.7×10^4

in terms of a compensated n -type semiconductor presented above accounts for the data at $T \geq 4$ K. Below 4 K, the data deviate toward a higher conductivity than is expected from an extension of the fit of Eq. (20) to lower temperatures, as is shown in Fig. 15(a). We ascribe the excess conductivity to originate in an additional conduction channel, resulting in

$$\sigma = \sigma_{\text{ex}} + \sigma_{\text{add}}. \quad (23)$$

Considering our description of the electrical transport outlined above, σ_{add} is identified as being due to conduction among the donor levels, contrary to σ_{ex} , which describes the conduction by electrons thermally activated from the donor levels to the conduction band. Conduction among donor levels is generally referred to as impurity or defect conduction. Depending on the donor or impurity concentration, different conduction mechanisms have been identified.⁵¹ While at low concentrations electron transport is thought to occur by hopping, higher concentrations allow for metallic conduction. Both features are usually identified by characteristic temperature dependences of $\sigma(T)$. In both cases the semiconductor has to be partially compensated, i.e., $0 < N_a/N_d < 1$, since otherwise the donor levels would be all filled or all empty at $T \rightarrow 0$. Our $\rho_{\text{add}} = 1/\sigma_{\text{add}}$ data cannot be described by a hopping-type temperature dependence⁵¹

$$\rho = \rho_0 \exp(T_0/T)^p, \quad (24)$$

but rather by

$$\rho = \rho_0 - AT^2 \quad (25)$$

below 0.3 K. In order to estimate whether the formation of a metallic band from our N_d donor levels is a reasonable scenario, we may use Mott's criterion for the metal-insulator transition in an impurity band,

$$n^{1/3} a_B \geq 0.25, \quad (26)$$

with the effective Bohr radius

$$a_B = \frac{\epsilon_{\text{eff}}}{m_n^*} \times 0.53 \text{ \AA}. \quad (27)$$

For $n = N_d = 10^{24} \text{ m}^{-3}$, which corresponds to $m_n^* = 7.3$, we obtain $a_B \geq 25 \text{ \AA}$ or $\epsilon_{\text{eff}}/m_n^* \geq 47$. Using $\epsilon_{\text{eff}} = 380$, as above, results in $m_n^* \leq 8$. The Mott criterion is thus indeed fulfilled, and we can assume that the N_d donor levels form a metallic impurity band. In this scenario we have to attribute an extremely narrow bandwidth to this impurity band. Since the energy $E_d \approx 0.6 \text{ meV}$ may unambiguously be identified from $\sigma(T)$ [see Fig. 15(a)], the impurity band is expected to be narrower or at most equal to this energy. We would like to mention in this connection that extremely narrow impurity bands can result from renormalization effects in correlated insulators.

The donor concentration $N_d = 10^{24} \text{ m}^{-3}$, which corresponds to 25 ppm, is orders of magnitude lower than the Kondo hole concentration of 9.9% given by Schlottmann and Hellberg²⁹ as an upper bound for a dirty Kondo insulator to become a metal. Whether the appearance of metallic behavior might alternatively be explained by a very small overlap of the valence and the conduction band—a local closing of

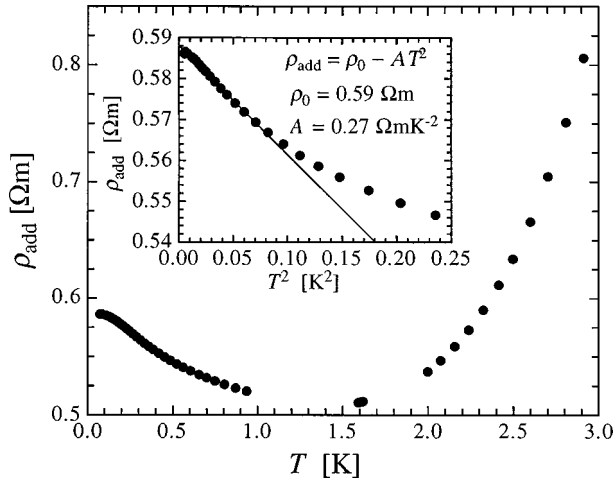


FIG. 17. Resistivity $\rho_{\text{add}}=1/\sigma_{\text{add}}$ vs temperature T , evaluated as explained in the text.

the gap of FeSi in the vicinity of magnetic impurities was proposed by Jarlborg¹⁸—cannot be answered here.

As $T \rightarrow 0$, $N_d - N_a$ electrons are expected to be present in the impurity band. The charge-carrier concentration below 1 K extracted from our Hall-effect data is approximately $2 \times 10^{22} \text{ m}^{-3}$. For $m_n^* = 7.3$, we have $N_d - N_a \approx 3 \times 10^{23} \text{ m}^{-3}$, and smaller values for higher effective-mass ratios. For $m_n^* \geq 10$, $N_a/N_d = 1$ within the error bars of the $\sigma(T)$ fit. The electron density derived from the Hall-effect measurements below 1 K is thus compatible with our interpretation of the transport data at higher temperatures.

In Fig. 17 we show ρ_{add} as a function of temperature for $T \leq 3$ K. Upon lowering the temperature, ρ_{add} first decreases, then passes through a minimum at approximately 1 K, and finally increases again. Below 0.3 K, $\rho = \rho_0 - AT^2$ is an adequate description of the data, as shown in the inset of Fig. 17. In view of $\rho_0 = 0.59 \text{ } \Omega \text{ m}$ the parameter $A = 0.27 \text{ } \Omega \text{ mK}^{-2}$ is extremely large.

The low temperature part of the specific heat is replotted in Fig. 18. The Schottky-type anomaly corresponds to an entropy release from approximately 0.1% two-level centers per FeSi unit with an energy separation of 0.95 K. This low

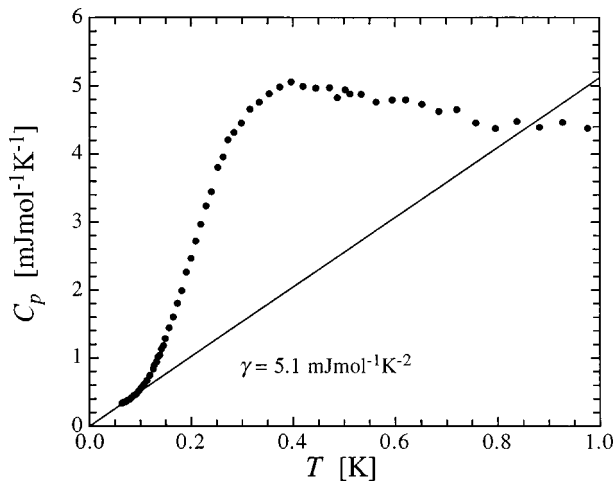


FIG. 18. Specific heat C_p of FeSi sample No. 2 as a function of temperature T below 1 K.

characteristic temperature may be indicative of the very narrow resonance of correlated electron states. At $T \leq 0.1$ K, $C_p(T)$ may be approximated by

$$C_p = \gamma T, \quad (28)$$

with $\gamma = 5.1 \text{ mJ mol}^{-1} \text{ K}^{-2}$. The power-law dependence of $\rho_{\text{add}}(T)$ and the linear-in- T contribution to the specific heat are indications for a metallic ground state. The density of states extracted from $\gamma = 5.1 \text{ mJ mol}^{-1} \text{ K}^{-2}$ is 8.7 states/eV/cell. Together with the density of itinerant electrons estimated from the Hall-effect measurements, $n \approx 2 \times 10^{22} \text{ m}^{-3}$, an effective-mass ratio of approximately 900 is derived, suggesting that the metallic ground state is highly correlated. In fact, the low-temperature behavior of $\rho_{\text{add}}(T)$ and $C_p(T)$ described above is reminiscent of what is encountered in single-impurity Kondo systems. The dominant contribution to the magnetic susceptibility between 100 and 1 K has a Curie-Weiss-type form, with a negative value of Θ , a behavior that is typically observed in Kondo systems above the Kondo temperature. As $T \rightarrow 0$ the susceptibility saturates in systems where a full moment compensation by conduction electrons is possible. Our $\chi(T)$ data, however, diverge as $T \rightarrow 0$, which indicates that the ground state is not fully spin compensated. Also, the hysteresis in the Hall effect below 1 K indicates that the ground state of FeSi is not a simple one. Part of the magnetic moments must be interacting to explain this phenomenon. On the other hand, there are also magnetic moments which remain paramagnetic down to at least 50 mK, as inferred from the $\chi(T)$ data. Such a mixed ground state is also observed in semimagnetic semiconductors, see e.g., Ref. 52. It seems that due to disorder and a low concentration of itinerant charge carriers, the competition between the various interaction mechanisms cannot clearly be resolved.

V. SUMMARY AND CONCLUSION

We have established a comprehensive data base for FeSi, performing measurements of the conductivity at temperatures between 0.07 and 300 K, the specific heat between 0.05 and 35 K, the magnetic susceptibility between 0.05 and 330 K, the optical reflectivity between 10 and 300 K in the spectral range from 15 to 10^5 cm^{-1} , the magnetoresistance at 7 T between 0.07 and 300 K, the magnetoresistance and Hall effect in varying fields up to 7 T between 2 and 55 K and between 0.07 and 55 K, respectively, and the magnetization in varying fields up to 5 T between 1.9 and 11 K. For all measurements, two single-crystalline samples were used which were grown by vapor transport during the same run and which were characterized by EDX and x-ray diffraction to be of high structural and chemical quality.

We tried to establish a physical picture for FeSi which is consistent with all these data, arriving at the following scenario. FeSi is a semiconductor with an unconventional band structure. The relevant energy gap is surrounded by pronounced peaks in the total DOS with a width of several 10 meV and a height of several 100 states/eV/cell. Each of the peaks contains four states per Fe site. The density-of-states effective-mass ratio characterizing the total DOS is of the order of 100. There appears to be an indirect gap relevant for electrical-transport measurements of 55–70 meV, and a

slightly larger direct gap of 75 to 100 meV for both charge and spin excitations. The precise value of the gap width depends on the precise shape of the assumed DOS. The conductivity effective mass ratio, characterizing the curvature in k space of the conduction band (valence band) at the energy minimum (maximum), is of the order of 10.

A comparison with local-density-approximation band-structure calculations shows that the qualitative agreement is good, but that significant discrepancies occur in the absolute values. The peaks in the total DOS next to the gap derived from experiment are higher by a factor of order 10 but of similar width, and the energy dispersion around the minima (maxima) of the conduction band (valence band) are a factor of order 10 flatter than predicted by the calculations. Whether these discrepancies are due to correlation effects—in particular on-site correlations are not properly accounted for by mean-field calculations—remains in our opinion a striking open question. The model of Fu and Doniach¹² for a strongly correlated insulator yields at least the correct tendencies, i.e., a flattening of the dispersion of the quasiparticle energy and a renormalization of the gap width and of the quasiparticle peaks upon increasing the Hubbard correlation energy U .

We also spent considerable effort on the analysis and interpretation of the low-temperature properties, which previously have frequently been classified as extrinsic and thus unimportant. Defects can, however, be useful even in analysing intrinsic properties of a semiconductor. The high-

temperature intrinsic-semiconductor description finds its extension to lower temperatures in the assumption of approximately 10^{24}-m^{-3} donor levels situated less than 1 meV below the conduction-band edge, and of a slightly lower acceptor concentration. These “impurities” are most likely coordinational defects in the perfect FeSi structure that might be related to a slight Si deficiency. Acceptors and ionized donors carry magnetic moments. While the mobility of the charge carriers is compatible with acoustic phonon scattering in the range of intrinsic conduction, it is very low in the range of extrinsic conduction, where the charge carriers appear to be interacting and weakly localized. At the lowest temperatures, FeSi exhibits features of a strongly correlated metal with a density of itinerant charge carriers of the order of only 10^{22} m^{-3} , which coexist with interacting magnetic moments. A possible origin of this metallic behavior is an impurity band formed out of the donor states, with a spectacularly narrow band width.

ACKNOWLEDGMENTS

We thank P. Wägli for the EDX investigation and H. Thomas for technical assistance. One of us (L.D.) is grateful to P. Wachter for generously providing infrastructural support. Part of this work was financially supported by the Schweizerischer Nationalfonds zur Förderung der Wissenschaftlichen Forschung.

-
- ¹G. Föex, *J. Phys. Radium* **9**, 37 (1938).
- ²V. Jaccarino, G. K. Wertheim, J. H. Wernick, L. R. Walker, and S. Aarj, *Phys. Rev.* **160**, 476 (1967).
- ³H. Watanabe, H. Yamamoto, and K. Ito, *J. Phys. Soc. Jpn.* **18**, 995 (1963).
- ⁴G. K. Wertheim, V. Jaccarino, J. H. Wernick, J. A. Seitchik, H. J. Williams, and R. C. Sherwood, *Phys. Lett.* **18**, 89 (1965).
- ⁵Y. Takahashi and T. Moriya, *J. Phys. Soc. Jpn.* **46**, 1451 (1979).
- ⁶Y. Takahashi, M. Tano, and T. Moriya, *J. Magn. Magn. Mater.* **31**, 329 (1983).
- ⁷S. N. Evangelou and D. M. Edwards, *J. Phys. C* **16**, 2121 (1983).
- ⁸G. Aeppli and Z. Fisk, *Comments Condens. Matter Phys.* **16**, 155 (1992).
- ⁹Z. Schlesinger, Z. Fisk, H.-T. Zhang, M. B. Maple, J. F. DiTusa, and G. Aeppli, *Phys. Rev. Lett.* **71**, 1748 (1993).
- ¹⁰Z. Fisk, J. L. Sarrao, J. D. Thompson, D. Mandrus, M. F. Hundley, A. Migliori, B. Bucher, Z. Schlesinger, G. Aeppli, E. Bucher, J. F. DiTusa, C. S. Oglesby, H. R. Ott, P. C. Canfield, and S. E. Brown, *Physica B* **206-207**, 798 (1995).
- ¹¹C. M. Varma, *Phys. Rev. B* **50**, 9952 (1994).
- ¹²C. Fu and S. Doniach, *Phys. Rev. B* **51**, 17 439 (1995).
- ¹³V. I. Anisimov, S. Y. Ezhov, I. S. Elfimov, I. V. Solov'yev, and T. M. Rice, *Phys. Rev. Lett.* **76**, 1735 (1996).
- ¹⁴T. Jarlborg, *Phys. Rev. Lett.* **77**, 3693 (1996).
- ¹⁵L. F. Mattheiss and D. R. Hamann, *Phys. Rev. B* **47**, 13 114 (1993).
- ¹⁶C. Fu, M. P. C. M. Krijn, and S. Doniach, *Phys. Rev. B* **49**, 2219 (1994).
- ¹⁷V. R. Galakhov, E. Z. Kurmaev, V. M. Cherkashenko, Y. M. Yarmoshenko, S. N. Shamin, A. V. Postnikov, S. Uhlenbrock, M. Neumann, Z. W. Lu, B. M. Klein, and Z.-P. Shi, *J. Phys.: Condens. Matter* **7**, 5529 (1995).
- ¹⁸T. Jarlborg, *Phys. Rev. B* **51**, 11106 (1995).
- ¹⁹G. E. Grechnev, T. Jarlborg, A. S. Panfilov, M. Peter, and I. V. Svechkarov, *Solid State Commun.* **91**, 835 (1994).
- ²⁰A. Lacerda, H. Zhang, P. C. Canfield, M. F. Hundley, Z. Fisk, J. D. Thompson, C. L. Seaman, M. B. Maple, and G. Aeppli, *Physica B* **186-188**, 1043 (1993).
- ²¹B. C. Sales, E. C. Jones, B. C. Chakoumakos, J. A. Fernandez-Baca, H. E. Harmon, J. W. Sharp, and E. H. Volckmann, *Phys. Rev. B* **50**, 8207 (1994).
- ²²M. Mihalik, M. Timko, P. Samuely, N. Tomašovičová-Hudáková, P. Szabó, and A. A. Menovsky, *J. Magn. Magn. Mater.* **157/158**, 637 (1996).
- ²³P. Samuely, P. Szabó, M. Mihalik, N. Hudáková, and A. A. Menovsky, *Physica B* **218**, 185 (1996).
- ²⁴L. Degiorgi, M. B. Hunt, H. R. Ott, M. Dressel, R. J. Feenstra, G. Grüner, Z. Fisk, and P. Canfield, *Europhys. Lett.* **28**, 341 (1994).
- ²⁵E. Bauer, S. Bocelli, R. Hauser, F. Marabelli, and R. Spolenak, *Physica B* **230-232**, 794 (1997).
- ²⁶R. Jullien and R. M. Martin, *Phys. Rev. B* **26**, 6173 (1982).
- ²⁷P. Schlottmann, *Phys. Rev. B* **46**, 998 (1992).
- ²⁸P. Schlottmann, *J. Appl. Phys.* **75**, 7044 (1994).
- ²⁹P. Schlottmann and C. S. Hellberg, *J. Appl. Phys.* **79**, 6414 (1996).
- ³⁰M. Hansen and K. Anderko, *Constitution of Binary Alloys* (McGraw-Hill, New York, 1958).
- ³¹M. B. Hunt, M. A. Chernikov, E. Felder, H. R. Ott, Z. Fisk, and

- P. Canfield, *Phys. Rev. B* **50**, 14 933 (1994).
- ³²E. Arushanov, C. Kloc, H. Hohl, and E. Bucher, *J. Appl. Phys.* **75**, 5106 (1994).
- ³³R. C. O'Handley, in *The Hall Effect and its Applications*, edited by C. L. Chien and C. R. Westgate (Plenum, New York, 1980), p. 417.
- ³⁴E. L. Nagaev, in *Physics of Magnetic Semiconductors* (MIR, Moscow, 1983), pp. 182 and 360.
- ³⁵G. P. Zinov'eva, L. P. Andreeva, and P. V. Gel'd, *Phys. Solid State* **23**, 711 (1974).
- ³⁶S. Takagi, H. Yasuoka, S. Ogawa, and J. H. Wernick, *J. Phys. Soc. Jpn.* **50**, 2539 (1981).
- ³⁷M. A. Chernikov, L. Degiorgi, E. Felder, S. Paschen, A. D. Bianchi, H. R. Ott, J. L. Sarrao, Z. Fisk, and D. Mandrus, *Phys. Rev. B* **56**, 1366 (1997).
- ³⁸H. Ohta, S. Kimura, E. Kulatov, S. V. Halilov, T. Nanba, M. Motokawa, M. Sato, and K. Nagasaka, *J. Phys. Soc. Jpn.* **63**, 4216 (1994).
- ³⁹A. Damascelli, K. Schulte, D. van der Marel, M. F ath, and A. A. Menovsky, *Physica B* **230-232**, 787 (1997).
- ⁴⁰E. Bauer, F. Marabelli, and R. Spolenak (private communication).
- ⁴¹D. Mandrus, J. L. Sarrao, A. Migliori, J. D. Thompson, and Z. Fisk, *Phys. Rev. B* **51**, 4763 (1995).
- ⁴²J. S. Blakemore, *Semiconductor Statistics* (Pergamon, Oxford, 1962).
- ⁴³K. Seeger, *Semiconductor Physics* (Springer-Verlag, Wien, 1973).
- ⁴⁴P. Nyhus, S. L. Cooper, and Z. Fisk, *Phys. Rev. B* **51**, 15 626 (1995).
- ⁴⁵B. L. Al'tshuler, A. G. Aronov, A. I. Larkin, and D. E. Khmel'nitskiĭ, *Zh. Eksp. Teor. Fiz.* **81**, 768 (1981) [*Sov. Phys. JETP* **54**, 411 (1981)].
- ⁴⁶A. Kawabata, *Solid State Commun.* **34**, 431 (1980).
- ⁴⁷A. I. Larkin, *Pis'ma Zh. Eksp. Teor. Fiz.* **31**, 239 (1980) [*JETP Lett.* **31**, 219 (1980)].
- ⁴⁸P. A. Lee and T. V. Ramakrishnan, *Rev. Mod. Phys.* **57**, 287 (1985).
- ⁴⁹J. C. Ousset, S. Askenazy, H. Rakoto, and J. M. Broto, *J. Phys. (Paris)* **46**, 2145 (1985).
- ⁵⁰D. V. Baxter, R. Richter, M. L. Trudeau, R. W. Cochrane, and J. O. Strom-Olsen, *J. Phys. (France)* **50**, 1673 (1989).
- ⁵¹B. I. Shklovskii and A. L. Efros, *Electronic Properties of Doped Semiconductors* (Springer-Verlag, Berlin, 1984).
- ⁵²R. R. Galazka and J. Kossut, in *Narrow Gap Semiconductors*, edited by W. Zawatzki, *Lecture Notes in Physics* Vol. 133 (Springer-Verlag, Berlin, 1980), p. 245.